COBEM 2021 26th International Congress of Mechanical Engineering
November 22-26, 2021, Virtual Congress, Brazil

COB-2021-1089
MODELING AND STRUCTURAL ANALYSIS OF AN ACADEMIC SHOCK TUBE

William Henrique de Lima Fiuza
George Santos Marinho
Paulo Gilberto de Paula Toro
João Carlos Arantes Costa Júnior
Universidade Federal do Rio Grande do Norte (UFRN). Centro de Tecnologia. Av. Senador Salgado Filho, 3000 - Campus Universitário, Lagoa Nova CEP 59.078-970 – Natal/RN - Brasil
william.fiuza.mec@gmail.com, gmarinho@ct.ufrn.br, toro11pt@gmail.com, arantes_jr@yahoo.com.br

Israel da Silveira Rêgo
Instituto de Estudos Avançados (IEAv). Divisão de Aerotermodinâmica e Hipersônica. Trevo Coronel Aviador José Alberto Albano do Amarante, nº1. Putim. CEP. 12.228-001. São José dos Campos/SP – Brasil
regoisrael@hotmail.com

Abstract. *The shock tube was created at the end of the 19th century for laboratory studies involving different areas of science, and in the mid-1950s it began to be used to simulate flight conditions, presented in high-speed flows. Such equipment has been widely adopted for laboratory hypersonic studies since then, as it provides accurate flow data as spacecraft will find in the atmosphere. Simple shock tubes consist of two sessions with a constant area, one high pressure (driver) and one low pressure (driven), the latter the testing session, axially joined and separated by one or two diaphragms. The rupture of the diaphragm produces an axial pressure gradient that causes the propagation of an incident shock wave in the direction of the driven tube, which is later reflected at the end of this session. The present paper shows the modeling and structural analysis of an academic shock tube, considering its joints, supports and efforts during the tests. The correct dimensioning of the components is essential, as it is equipment that works with high pressures and different gases, in order to avoid accidents and errors in the information obtained in tests. Therefore, it is necessary to model all components in CAD (Computer Aided Design) and CAE (Computer Aided Engineering) softwares, with subsequent discretization by mesh generation and computational structural analysis by Finite Element Method. Boundary conditions and applied loads must be correctly selected for a good level of confidence in the computational analysis. The choice of materials for the fixing screws, flanges and supports is also addressed during this work, based on economic, mechanical factors, and the feasibility of finding and acquiring such materials. The project is expected to be reliable, academically useful, and economically optimized so that in the future it can be used at the university level, benefiting and encouraging students in the aerospace and mechanical sciences.*

Keywords: *shock tube, shock tube modeling, numerical structural analysis.*

1. INTRODUCTION

The simplest shock tube consists of two reservoirs (driver and driven tubes), with the constant cross section area, separated by a single thin diaphragm. The diaphragm allows maintaining different pressure in each tube. Different gases at different temperatures can be used in the driver and driven sections, as shown in Figure 1.

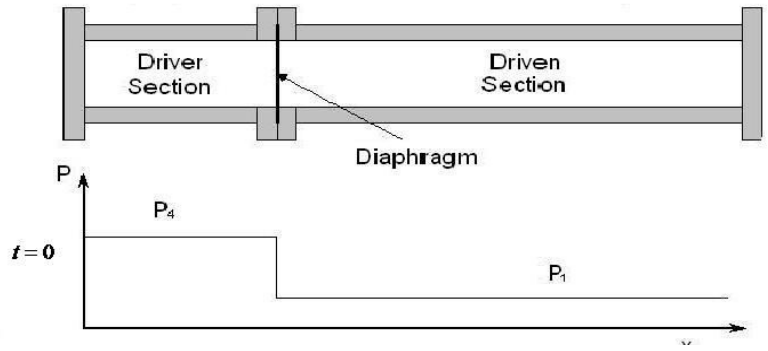

Figure 1. Constant cross section area Shock Tube, initial conditions (Mantovani et al., 2011).

In 1899, the first shock tube was constructed by Paul Vieille, where the driver (high pressure) and driven (low pressure) tubes were 6-meter long and 22 mm diameter. The test section was 271 mm, placed at the end of the driven tube. Cellophane, paper, and metal foil were used as the diaphragm materials. Driver and driven tubes were pressurized with air at 27 atm and at 16 atm, respectively. Cellophane diaphragm, from 0.11 mm and 0.29 mm thicknesses, were used to establish the incident shock, with Mach number 2, in the driven tube (Fomin, 2010). Since then, the Shock Tubes have been used extensively to investigate many special problems that arise in various fields such as chemistry, physics, fluid dynamics, structures, and astrophysics.

As early as 1950, Nagamatsu realized the severe enthalpy and Mach number limitations of steady-state hypersonic wind tunnels. As a result, Yoler (1954) and his Advisor Prof. Dr. Nagamatsu, designed a shock tube, with a nozzle attached to the end wall of the driven tube, to drive the hypersonic flow of air in a nozzle, to produce higher flow Mach numbers with higher stagnation temperatures in the test section, as shown in Figure 2. Based on the very promising results obtained, Nagamatsu et al. (1959), a few years later, designed and built the General Electric 24-in. and 48-in. diameter combustion driver Hypersonic Shock Tunnel. The General Electric 24-in. diameter Hypersonic Nozzle and Dump Tank used was deactivated and donated to Rensselaer Polytechnic Institute (RPI).

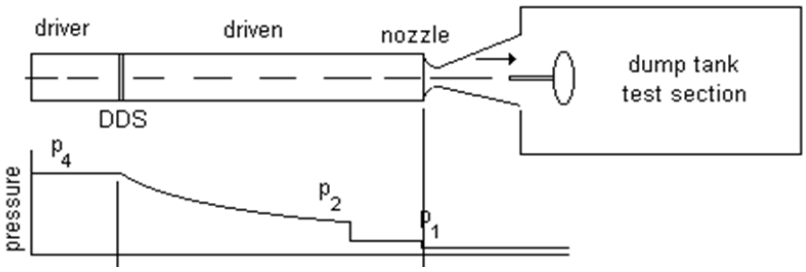

Figure 2. Hypersonic Shock Tunnel (Romanelli Pinto et al., 2011; Toro, 1998).

Therefore, since 1950s, shock tubes and shock tunnels are the most versatile experimental ground test facilities to simulate the high velocity and high temperature (high enthalpy) conditions encountered during the space vehicle reentry into the Earth's atmosphere, for very short times, in the test section, a uniform hot gas flow, from 50 microseconds to 10 milliseconds, using specialized measurement techniques to obtain reliable pressure and temperature (heat flux) data (Nagamatsu, 1958; 1961; Nagamatsu et al.,1959).

The RPI 4-in (101.6 mm) diameter low pressure Shock Tube was constructed, where the driver and driven tube's material was a thin-walled copper pipe with 4-in internal diameter and 0.10-in (2.54 mm) wall thickness. The driver and driven tubes are 10-ft (3.048 m) long and 60-ft (18.288 m) long, respectively. The test section was placed either at the end of the driven tube. Instrumentation ports as well as load and/or vacuum ports are provided along the tube. These ports were used mainly to install the pressure transducers to measure the shock wave strength and to monitor the shock wave transit time (Minucci, 1991; Toro, 1998).

The RPI 24-in (0.6096 m) diameter Hypersonic Shock Tunnel was used for low and high enthalpy stagnation conditions. This facility was capable of generating reservoir enthalpies up to 6.5 MJ/kg (4100 K) when operating in the Equilibrium Interface Mode with Helium in the driver tube. Mach numbers from 10 to 25 with stagnation temperature less than 1000 K can be achieved for low enthalpy case, where no dissociation is assumed and the perfect gas equation may be used. However, with temperatures higher than 1000 K, dissociation, ionization or even recombination can occur, and the perfect gas equation cannot be considered. The real gas effects must be taken into account for a high enthalpy case with Mach number range of 8 to 20 in the test section can be achieved with a particular value of stagnation temperature of 4100 K and helium as a driver gas at 1950 psi (133 atm) (Minucci, 1991; Toro, 1998).

Based upon the experience obtained by its designers (Minucci and Toro) in operating the Ressenlaer Polytechnic Institute (RPI), the Hypersonic High Enthalpy Real Gas Pulsed Reflected Shock Tunnel, funded, in 2005, by the Fundação de Amparo à Pesquisa do Estado de São Paulo (FAPESP), was designed as Research and Development facility for basic investigations in supersonic combustion applied to high-speed advanced airbreathing propulsion, for basic electromagnetic energy addition for external flow control and for general aerothermodynamics applied in conventional aerospace vehicle. The Hypersonic Shock Tunnel was installed at the Laboratory of Aerothermodynamics and Hypersonics of Prof. Henry T. Nagamatsu, at Instituto de Estudos Avançados (IEAv). The IEAv 0.60-m nozzle exit diameter hypersonic shock tunnel was designed for long test times, 2-10 milliseconds, suitable for the experiments performed at the laboratory. Free stream Mach numbers ranging from 6 to 25 can be produced and stagnation pressures and temperatures up to 360 atm. and up to 9,000 K, respectively, can be generated. Shadowgraph and schlieren optical techniques have been used for flow visualization (Toro et al., 2005; 2007).

MSC NASTRAN, 2005 version, was used to structural analysis the high and the low pressure reservoirs, the nozzle coupled to test section (dump tank), where the incident and reflected shock wave travels from the driver to the dump tank, during the shock tunnel operation (Pereira, 2005). In 2018, based in the shock tube operation, a numerical and

analytical methodologies were applied to structural analysis of the, realistic, high (driver) pressure reservoir of a shock tube, including flanges and screws (Rodrigues, 2018).

2. SHOCK TUBE OPERATION AND FLOW MODELING

2.1 Shock Tube operation

Initially, both driver and driven sections are separated by a diaphragm, which bursts at the select high pressure in the driver tube. The driver section is filled with a driver gas, at an initial high pressure p_4, and an ambient temperature T_4. The driven section is filled with a driven gas, at an initial low pressure p_1, and an ambient temperature T_1. Different gases at different temperatures may be used in the driver and driven sections. An unsteady one-dimensional strong normal shock wave is established after the diaphragm breaks, at the selected high pressure in the driver section. The shock wave propagates through downstream of the driven low pressure section, with velocity u_s, and compresses the flow to a pressure p_2 at temperature T_2, and induces a mass motion with velocity, u_2. In this case, all flow properties p(x,t), ρ(x,t), T(x,t), u(x,t), depend on both space (x) and time (t). At the same running time, an expansion wave propagates upstream into a high pressure driver section, reducing, smoothly and continuously, the pressure from the initial values p_4 and T_4 to p_2 and T_2. Ideal diaphragm opening and ideal wave behavior should be assumed (no damping, no viscous boundary layer effects). Behind the primary shock wave, a contact surface, which separates the driven gas and the driver gas, propagates downstream in the driven section. Across the contact surface, the velocity and the pressure are equal for both driven and driver gases, but, in general the temperature and the density may not be. A few milliseconds after the bursting of the main diaphragm, the primary shock wave arrives at the end wall of the driven section. In this time, a reflected shock wave is established. After opening the diaphragm, the flowfield is completely determined by a given condition in the driver and driven sections, before the main diaphragm is broken, and perfect gas may be assumed for relatively low temperatures. For high temperatures, where the perfect gas is no longer valid, the real gas effects modify the results for shock tube flow (Mantovani et al., 2011; Romanelli Pinto et al., 2011).

2.2 Shock Tube flow modeling

The one-dimensional incident strong normal shock wave moving into a stationary (driven) gas and the reflect shock wave mode (Anderson, 2003; Minucci, 1991; Toro, 1998, Mantovani et al., 2011; Romanelli Pinto et al., 2011) may be used to calculate the flow conditions in the shock tube and the flow over the test model, shown in Figure 1, placed at the end of the shock tube, and the governing flow equations for the one dimensional incident shock wave are given by

$$\rho_1 u_S = \rho_2 (u_S - u_2) \tag{1}$$

$$p_1 + \rho_1 {u_S}^2 = p_2 + \rho_2 (u_S - u_2)^2 \tag{2}$$

$$h_1 + \frac{1}{2}{u_S}^2 = h_2 + \frac{1}{2}(u_S - u_2)^2 \tag{3}$$

Once the conditions after the incident shock wave are determined, the conditions existing in the reflected shock wave can be found. The incident shock wave is totally reflected, so u_5 =0. The governing flow equations, for the one-dimensional reflected shock wave are given by

$$\rho_2 (u_2 + u_r) = \rho_5 u_r \tag{4}$$

$$p_2 + \rho_2 (u_2 + u_r)^2 = p_5 + \rho_5 {u_r}^2 \tag{5}$$

$$h_2 + \frac{1}{2}(u_2 + u_r)^2 = h_5 + \frac{1}{2}{u_r}^2 \tag{6}$$

If the conditions achieved in the shock tube are high enough to produce dissociation, ionization or even recombination, the real gas equation $h = h(p, \rho)$ must be used; otherwise the calorically perfect gas equation is used $p = \rho RT$, then the gas constant and the specific heat ratio given by $R = c_p - c_v$ and for gas $\gamma = c_p / c_v$, respectively; and the enthalpy given by $h = c_p T$.

For the calorically perfect gas assumption the incident, Eqs. (1-3), and the reflected, Eqs. (4-6), shock wave governing equations may be manipulated and one may find the closed analytical solutions (Nagamatsu, 1958; 1961;

Anderson, 2003, Minucci, 1991; Toro, 1998; Mantovani et al., 2011, Romanelli Pinto et al., 2011). For incident shock wave the closed analytical solutions are given by

$$\frac{p_2}{p_1} = \frac{2\gamma_1 {M_S}^2 - (\gamma_1 - 1)}{\gamma_1 + 1} \tag{7}$$

$$\frac{\rho_2}{\rho_1} = \frac{(\gamma_1 + 1){M_S}^2}{(\gamma_1 - 1){M_S}^2 + 2} \tag{8}$$

$$\frac{T_2}{T_1} = \frac{\left[2\gamma_1 {M_S}^2 - (\gamma_1 - 1)\right]\left[(\gamma_1 - 1){M_S}^2 + 2\right]}{(\gamma_1 + 1)^2 {M_S}^2} \tag{9}$$

where the incident shock wave Mach number is given by $M_S = \frac{u_S}{a_1}$ and $\gamma_1 = \frac{c_p}{c_v}$ is the ratio of the specific heats.

The induced velocity imparted by the shock wave moving at constant velocity u_2 may be determined by the continuity condition across the shock wave. Therefore, the induced Mach number M_2, after a moving normal shock wave, is given as function of the incident shock Mach number M_S, and they are given by

$$u_2 = \frac{2}{\gamma_1 + 1} u_S \left(\frac{{M_S}^2 - 1}{{M_S}^2}\right) = \frac{2}{\gamma_1 + 1} a_1 \left(M_S - \frac{1}{M_S}\right) \tag{10}$$

$$M_2 = \frac{2({M_S}^2 - 1)}{\sqrt{\left[(\gamma_1 - 1){M_S}^2 + 2\right]\left[2\gamma_1 {M_S}^2 - (\gamma_1 - 1)\right]}} \tag{11}$$

After the incident shock wave arrives at the end of the driven tube, the gas is brought to rest, the shock wave is reflected, and the temperature, the pressure and density of the gas after the reflected shock wave are increased, and similar as for incident shock relations, closed analytical solutions are given by

$$\frac{p_5}{p_2} = \frac{2\gamma_1 {M_r}^2 - (\gamma_1 - 1)}{\gamma_1 + 1} \tag{12}$$

$$\frac{\rho_5}{\rho_2} = \frac{(\gamma_1 + 1){M_r}^2}{(\gamma_1 - 1){M_r}^2 + 2} \tag{13}$$

$$\frac{T_5}{T_2} = \frac{\left[2\gamma_1 {M_r}^2 - (\gamma_1 - 1)\right]\left[(\gamma_1 - 1){M_r}^2 + 2\right]}{(\gamma_1 + 1)^2 {M_r}^2} \tag{14}$$

where, the reflected shock Mach number M_r is function only of the incident shock wave Mach number M_S, the ratio of specific heats γ_1 of the existent gas in the driven section, given by

$$\frac{M_r}{{M_r}^2 - 1} = \frac{M_S}{{M_S}^2 - 1} \sqrt{1 + \frac{2(\gamma_1 - 1)}{(\gamma_1 + 1)^2}({M_S}^2 - 1)\left((\gamma_1 + 1)\frac{1}{{M_S}^2}\right)} \tag{15}$$

Simultaneously, with the instantaneous opening of the diaphragm (between the high and low pressure reservoirs) a rarefaction wave propagates into the high pressure driver tube. The conditions relating the gas states on both sides of the contact surface are that the velocity and pressure are constant across the contact surface. They are given by $u_2 = u_3$ and $p_2 = p_3$. The driver to driven pressure ratio (Shock Tube relation) is given by

$$\frac{p_4}{p_1} = \frac{p_2}{p_1}\left\{1 - \left[\frac{a_1(\gamma_4 - 1)}{a_4(\gamma_1 + 1)}\right]\left[M_S - \frac{1}{M_S}\right]\right\}^{-\frac{2\gamma_4}{(\gamma_4 - 1)}} \tag{16}$$

3. ANALYSIS OF FLOW PROPERTIES

3.1 Theoretical analysis

Solving incident shock wave relations, Eqs. (7-10), for air as calorically perfect gas, as incident Mach number M_S goes to infinite ∞, the pressure and temperature ratios go to infinite, Figures 3 and 4, respectively. However, as incident Mach number M_S goes to infinite, the density ratio, Figure 5, approaches to a finite value 6, and the induced flow Mach number M_2, Figure 6, behind the non-stationary shock wave approaches to 1.89.

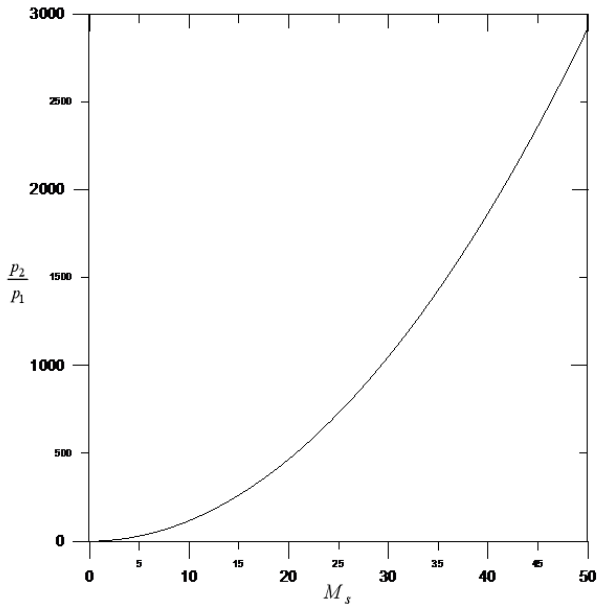

Figure 3. Pressure ratio across incident wave.

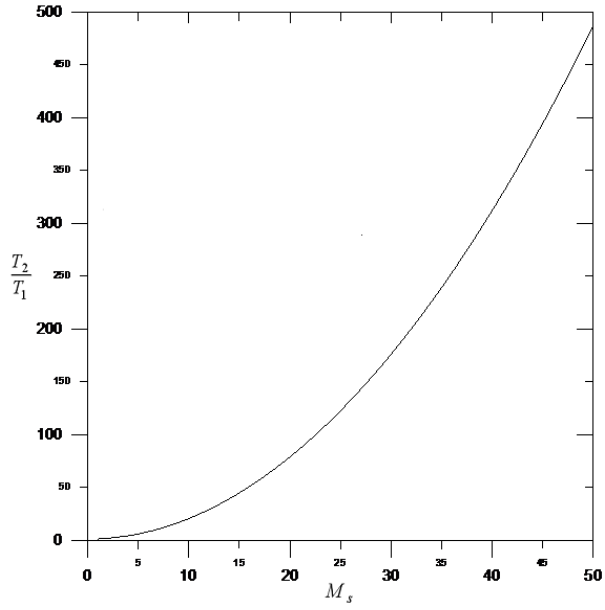

Figure 4. Temperature ratio across incident wave.

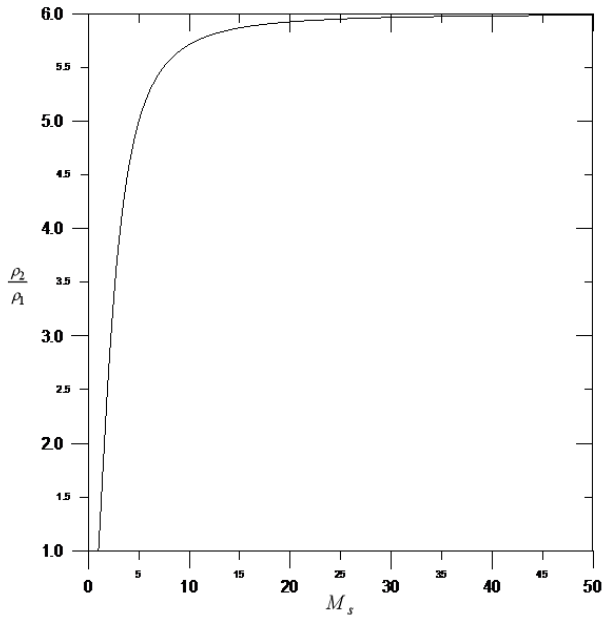

Figure 5. Density ratio across incident wave.

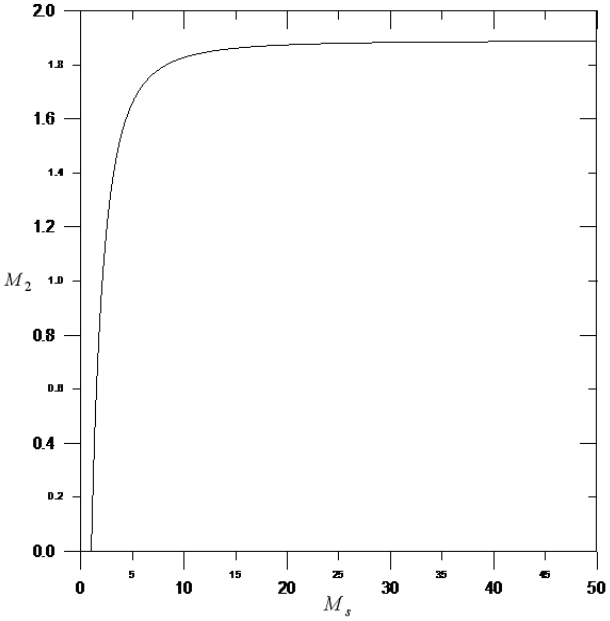

Figure 6. Mach number behind incident wave.

Similar to incident shock wave relations, solving reflected shock wave, Eqs. (12-15), as incident Mach number M_S goes to infinite ∞, the pressure and temperature ratios shown in Figures 7 and 8 go to infinite, but density ratio, in Figure 9, approaches to a finite value 21, and flow Mach number M_r, in Figure 10, behind the non-stationary shock wave approaches to 2.6.

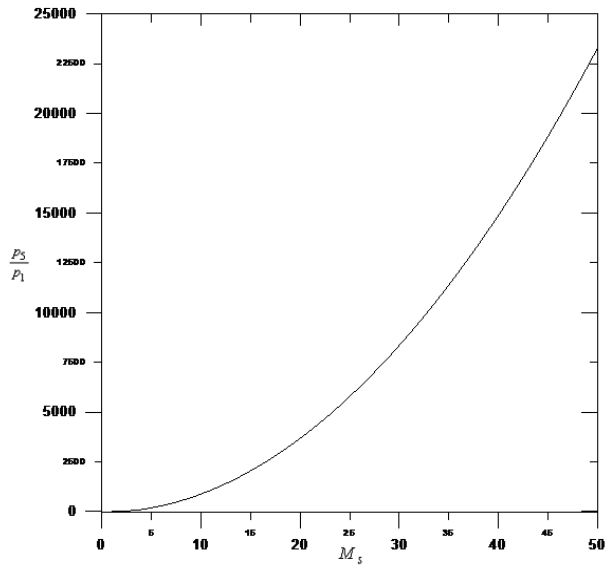

Figure 6. Pressure ratio across reflected wave.

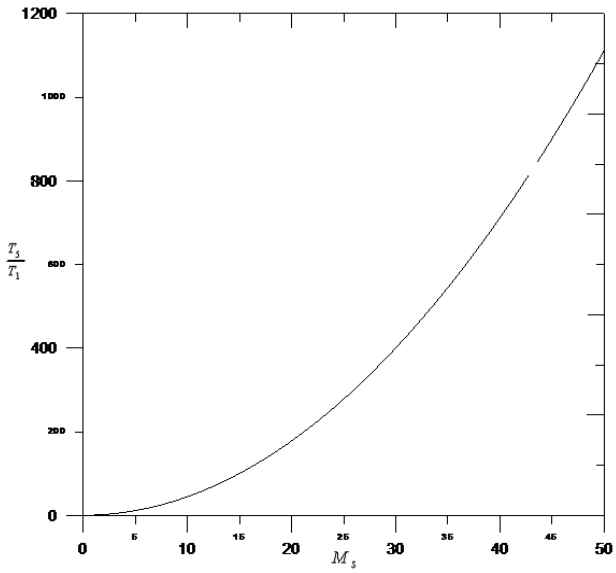

Figure 7. Temperature ratio across reflected wave.

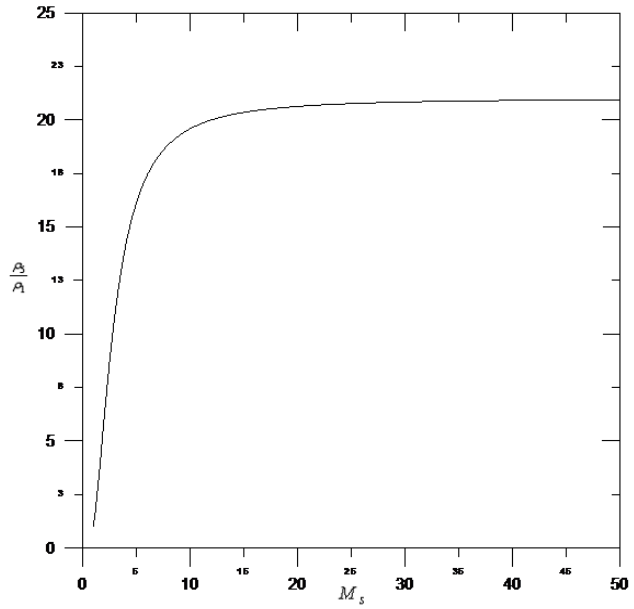

Figure 9. Density ratio across reflected wave.

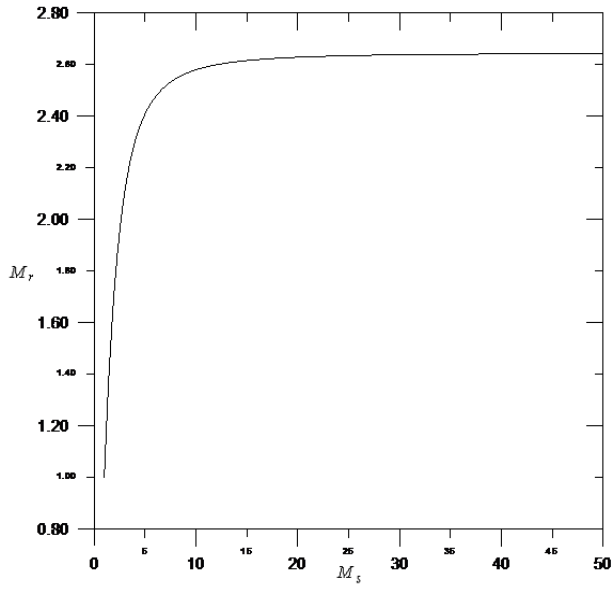

Figure 10. Mach number behind reflected wave.

Knowing the initial pressure conditions and the gases γ_4 and γ_1 involved, in the driver p_4 and driven p_1 sections, the driver to driven pressure ratio (diaphragm pressure ratio), p_4/p_1, Eq. (16), which determines the strengths of the incident shock and the expansion waves, those established after the diaphragm was broken, can determine the incident normal Mach number M_S. When the driver is pressurized with air and for a very high driver to driven pressure ratio, p_4/p_1, the maximum incident shock wave Mach number reach to approximately 6, as shown in Figure 11.

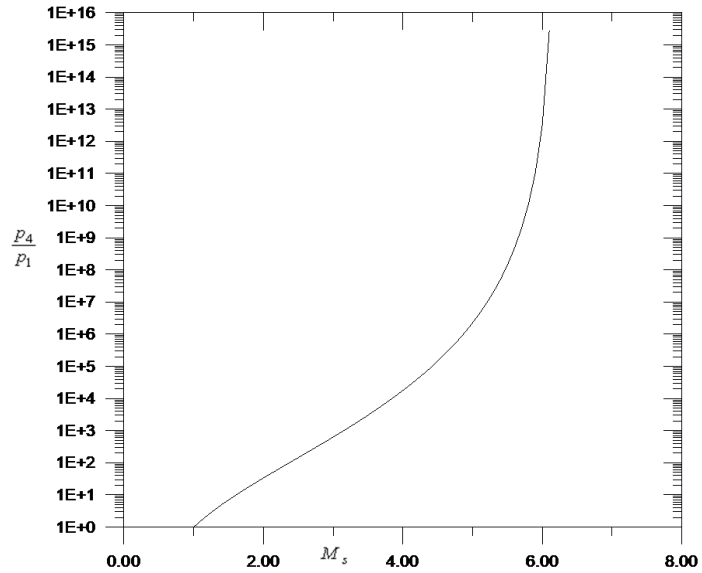

Figure 11. Pressure ratio across incident shock wave.

3.2 Computational structural analysis

According to Reddy (2006), mathematical models are the analytical description of physical phenomena and processes, being developed through assumptions about how the process works and employing governing laws. Because these laws are characterized by very complex differential and integral equations, before the possibility of using computers to solve the problems, the created models were simplified a lot, aiming at solving them in an analytical way.

From the moment computational technology develops enough to be applied in complex calculations, numerical simulations arise, with the application of numerical methods aimed at evaluating mathematical models. The Finite Element Method (FEM) is the most powerful tool to be applied in the analysis of practical engineering problems, and it is extremely important that it be applied properly. Such problems, with very complex domains geometrically and in the constitution of the materials used, in addition to the application of loads, can have their approximate solutions using FEM (Reddy, 2006).

4. METHODOLOGY

The driver section of the academic shock tube is represented three-dimensionally using Autodesk Inventor Professional 2020 software, as shown in Figure 12, with flanges being added to the ends, joined to the tube by a completely restricted and simplified joint. The measurements used in the model correspond to the measurements of the tubes that Universidade Federal do Rio Grande do Norte (UFRN) has, aiming at greater proximity to reality.

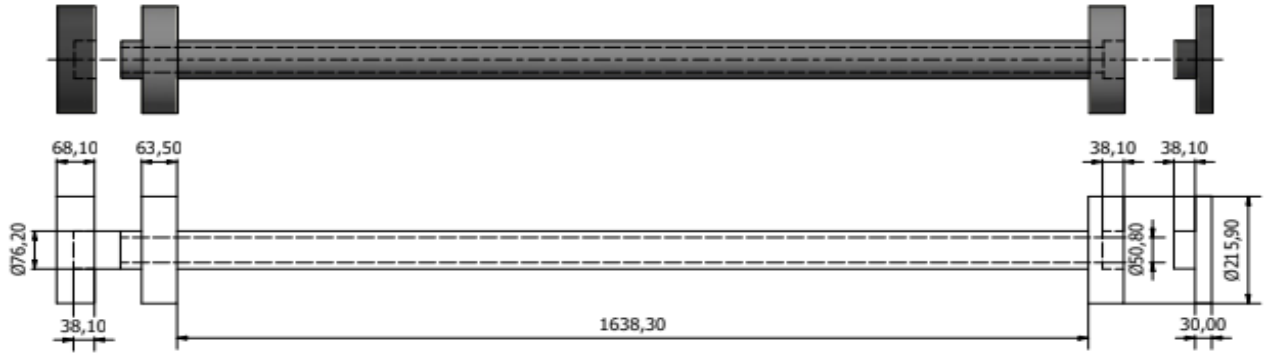

Figure 12. Shock tube section model with flanges and measurements represented in millimeters.

After creating the model, two meshes are generated, shown in Table 1, the first coarse and the second refined. Such methodology is adopted to enable the comparison of results between the two types of mesh. Below is a data table for model discretization.

Table 1. Mesh settings for model discretization.

	Average element size, mm (1)	Minimum size of elements, mm (2)	Leveling factor	Maximum turning angle	Create curved mesh elements
Mesh 1	0.01	0.1	1.5	60°	Yes
Mesh 2	0.004	0.1	1.5	60°	Yes

(1) fraction of model diameter
(2) fraction of average size

Considering that only the average size of the elements is changed between meshes 1 and 2, there is a considerable difference in the number of elements and nodes, reflecting later the computational results obtained through the Finite Element Method analysis. The first mesh has 24,041 nodes and 14,000 elements, while the second mesh has 271,771 nodes and 177,737 elements. In Figure 13, it is possible to visually notice the differences in the refinement of the generated meshes.

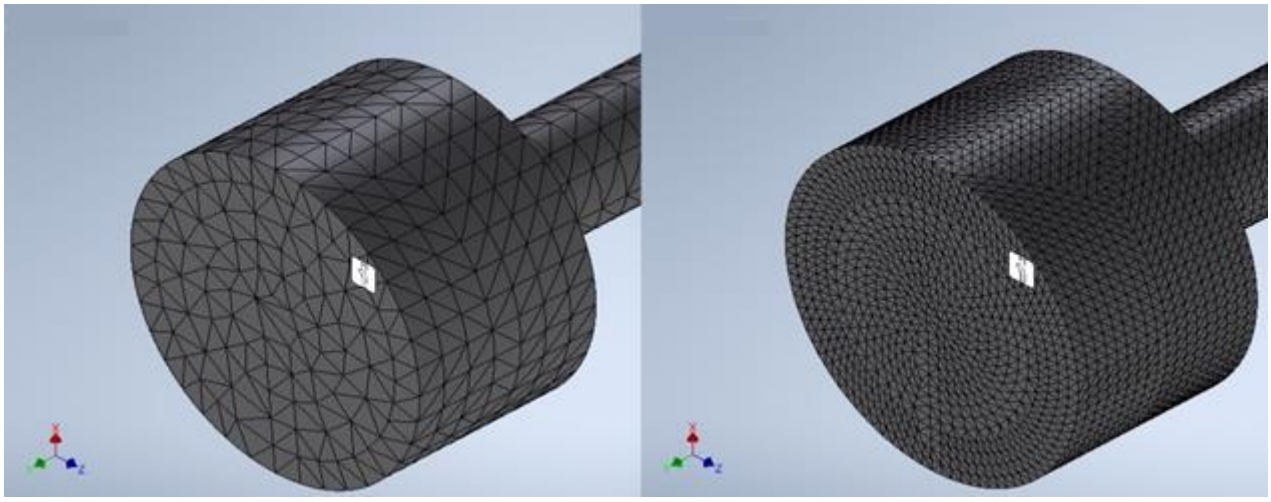

Figure 13. Partial views of generated meshes.

After the model discretization, it is necessary to use the characteristics of the materials used. To simplify the simulation and remain faithful to the real tube, stainless steel was used as the material, with the mass of the set being calculated and resulting in 97.0729 kg. The Table 2 shows the material and model properties used as a basis for computer simulations.

Table 2. Properties of material used and pipe measurements with flanges.

Density, kg/m^3	Area, m^2	Volume, m^3	Flow resistance, MPa	Maximum tensile strength, MPa	Young's Module, GPa	Poisson's Coefficient	Shear Modulus, GPa
8000	0.967971	0.0121341	250	540	193	0.30	74.2308

The loads exerted during the operation of an academic shock tube are considered during the structural analysis, and it is important to determine support points and surfaces that receive the load. For the simulation in question, an initial internal pressure (p_4) in the driver section equivalent to 100 atm, or 10.133 MPa, was assigned. Pressure is applied to the inner surface, shown in green in the figure below. Temperature (T), enthalpy (h) and Mach number (M) of the flow were not considered in the computational structural analysis performed. The flanges were fixed, simulating the fixation points of the equipment support, shown in Figure 14 as white squares.

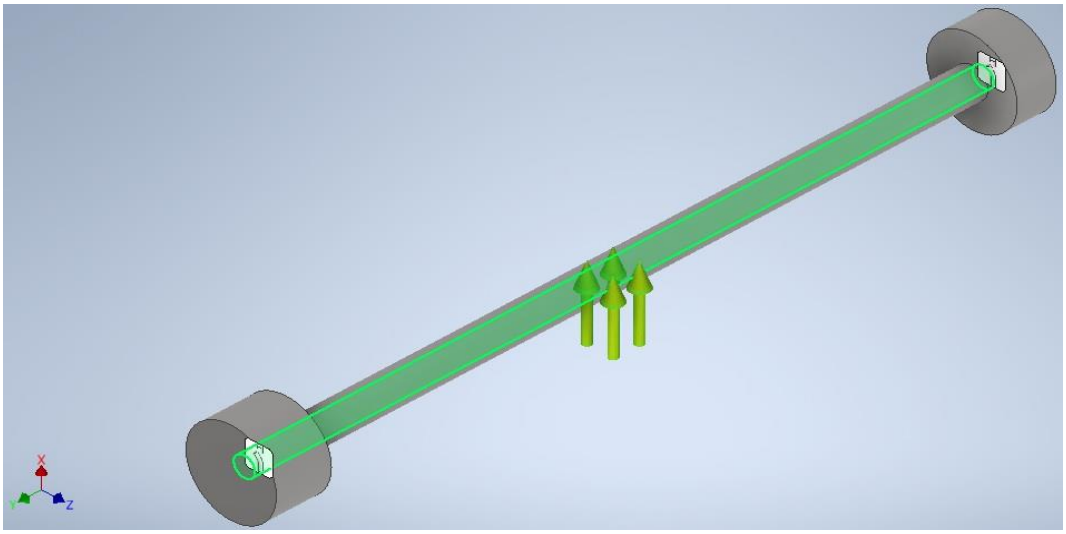

Figure 14. Pressure exerted and attachment points of the structure.

5. RESULTS AND COMMENTARIES

With simplified equipment modeling, meshing discretization and application of loads and constraints, the software has all the information needed for computer simulation. The factors calculated are the von Mises Stresses, displacements, and deformations that the structure undergoes in three dimensions, featuring an advantage over two-dimensional calculation methods, which greatly simplify the model and distance themselves from reality. Below, the Table 3 shows the differences between the results obtained through meshes 1 and 2.

Table 3. Results obtained for the two generated meshes.

	Minimum von Mises Stress, MPa	Maximum von Mises Stress, MPa	Minimum displacement, mm	Maximum displacement, mm	Minimum equivalent deformation	Maximum equivalent deformation
Mesh 1	0.0841421	35.1411	0	0.00412966	$3.9581\ 10^{-7}$	$1.58917\ 10^{-4}$
Mesh 2	0.0591384	33.3626	0	0.00410292	$2.7131\ 10^{-7}$	$1.51127\ 10^{-4}$

Note that the von Mises Stress varies considerably between the coarse mesh and the fine mesh, with a difference of 1.7785 MPa at the maximum point. The maximum displacement suffers a less noticeable change, with a difference of $2.674\ 10^{-5}$ mm.

If the mesh generated is continuously refined, the computer responsible for simulating the model will take longer and longer to calculate all the variables, as the number of elements and nodes increases considerably. As an example, if the average size of the elements is 0.001 mm, and all other information remains as in Table 1, the generated mesh will have more than 1.7 million nodes. In the following figures, graphic expressions of the results obtained with the two meshes initially proposed.

The factor of safety can be calculated as the ratio between the stress the material resists to the stress exerted on the material. Considering that the maximum stress that stainless steel withstands is equal to 540 MPa, and that the maximum stress obtained in the simulations is equal to 35.1411 MPa, the safety factor value of the high pressure section of the shock tube is approximately 15.36.

It can be seen through Figure 15 (a-b) that the deformation is equal to zero on the outer surfaces of the flanges, as they are the fixed points. Displacements are maximum near the flanges (red regions) and intermediate in the center area of the tube (green regions).

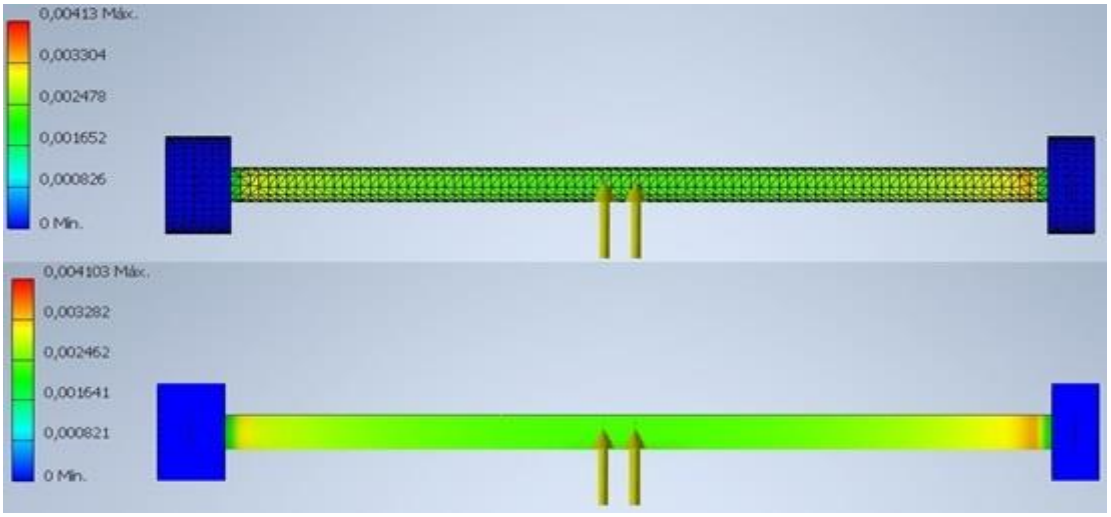

Figure 15. (a) Displacements suffered by the structure, data from the first mesh in millimeters (mm). (b) Displacements suffered by the structure, data from the second mesh in millimeters (mm).

In Figure 16 (a) and 16 (b) it is possible to evaluate the von Mises Stresses in the tubular structure, with such stresses being distributed in locations similar to those seen in the graphic representation of the displacements.

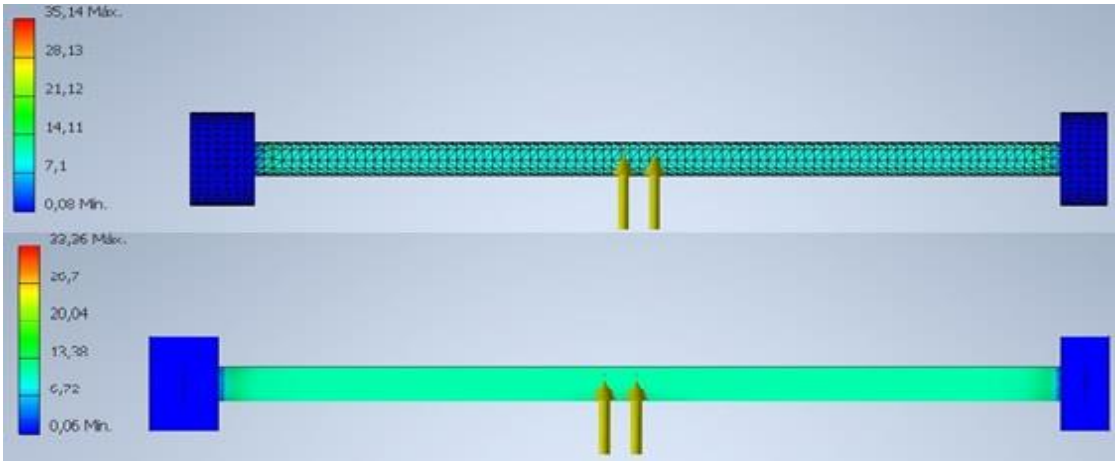

Figure 16. (a) von Mises Stress suffered by the structure, data from the first mesh in megapascal (MPa). (b) von Mises Stress suffered by the structure, data from the second mesh in megapascal (MPa).

With the results obtained, it can be stated that the tubes available to UFRN support the pressure loads exerted during its operation, as their resistance to flow, tension and shear modulus have values much higher than those obtained in the simulation.

6. CONCLUSIONS

The present work demonstrates, through the use of a computational tool, the possibility of building an academic shock tube based on the material available at the Universidade Federal do Rio Grande do Norte (UFRN), provided by Instituto de Estudos Avançados (IEAv). Simplified simulations are valid, given the brevity of this paper, but require further evaluations and calculations before building a prototype. In addition, economic factors must also be taken into consideration in the future, as the academic shock tube is an expensive equipment.

From this initial work, it is possible to improve the models in software to bring them closer to reality, until the prototype can be built safely and avoiding wasted work and material. Items such as the diaphragm between different sections, flange fixing screws and frame supports add complexity to the studies, but are strictly necessary for accurate sizing of the shock tube. These items can be added later in a more complex study.

It is worth noting that the results obtained show that the available material resists work pressure and can be used in the construction of the academic shock tube. However, before the prototype is manufactured, tests are needed to assess the integrity of the tubes, looking for possible cracks, manufacturing defects or any other types of damage. This

verification is important because the shock tube is an equipment that works with different pressures, which are much higher than atmospheric pressure, and any problem in the operation is potentially dangerous for the operator and for the laboratory.

7. ACKNOWLEDGEMENTS

This study was financed in part by the Coordenação de Aperfeiçoamento de Pessoal de Nível Superior - Brasil (CAPES) - Finance Code 001. Also, the authors would like to thank CAPES the support given by the Project PROCAD-DEFESA 88887.626266/2021-00. The authors would like to thank Universidade Federal do Rio Grande do Norte (UFRN) to support granted to carry out the Shock Tube structural design. The last author would like to extend his gratitude to Instituto de Estudos Avançados (IEAv) to encourage the collaboration between IEAv and UFRN.

8. REFERENCES

Anderson Jr., J. D., 2003. Modern Compressible Flow: with Historical Perspective. McGraw-Hill series in Aeronautical and Aerospace Engineering. Third Edition. ISBN O-07-242443-5. ISBN 0-07-1 12161-7 (ISE).

Fomin, N. A., 2010. 110 years of experiments on Shock Tubes. Journal of Engineering Physics and Thermophysics. Vol. 83, n. 6, p. 1118-1135.

Nagamatsu, H. T., 1958. Shock Tube Technology and Design. Report No. 58-RL-2107. General Electric Research Laboratory, Schenectady, New York.

Nagamatsu, H. T., Geiger, R. E. and Sheer, R. E. Jr., 1959. Hypersonic Shock Tunnel. ARS Journal, vol. 29, pp. 332-340.

Nagamatsu, H. T., 1961. Fundamental Data Obtained from Shock-Tube Experiments. Chapter III Shock Tube Technology and Design," Pergamon Press, Editor A. Ferri.

Mantovani, A. F., Romanelli Pinto D., Toro, P. G. P., Minucci, M. A. S., 2011. Shock Tube Operation, Flow Modeling and Theoretical Analysis. 21st Brazilian Congress of Mechanical Engineering. October 24-28, Natal, RN, Brazil.

Minucci, M. A. S.,1991. An Experimental Investigation of a 2-D Scramjet Inlet at Flow Mach numbers of 8 to 25 and Stagnation Temperatures of 800 to 4100 K. Doctoral Thesis, Rensselaer Polytechnic Institute, May 1991.

Pereira, A. L., 2006. Análise estrutural de um túnel de choque hipersônico. Dissertação de Mestrado. ITA.

Reddy, J. N., 2006. An Introduction to the Finite Element Method. Third Edition. McGraw-Hill, New York.

Rodrigues, V. E. B. (2018). Análise estrutural de um tubo de choque acadêmico. Trabalho de Graduação. UFRN.

Romanelli Pinto D., Marcos, T. V. C., Toro, P. G. P., Minucci, M. A. S., Oliveira, A. C., Chanes Junior, J. B. (2011). Preliminary Characterization of the Hypersonic Flow in the Test Section of the IEAv T3 Hypersonic Shock Tunnel. 21st Brazilian Congress of Mechanical Engineering. October 24-28, Natal, RN, Brazil.

Toro, P. G. P. (1998). Experimental Pressure and Heat Transfer Investigation over a Directed-Energy Air Spike Inlet at Flow Mach Numbers of 10 to 20, Stagnation Temperature of 1000 K, and Arc Power up to 127 KW. Ph.D Thesis, Rensselaer Polytechnic Institute, Troy, New York.

Toro, P. G. P., Minucci, M. A. S., Chanes Jr., J. B., Pereira, A. L. and Nagamatsu, H. T. (2005). Development of a New Hypersonic Shock Tunnel Facility to Investigate basic Supersonic Combustion and basic Electromagnetic Energy Addition for Flow Control. 4th International Symposium on Beamed Energy Propulsion, Japan.

Toro, P. G. P.; Minucci, M. A. S.; Chanes Jr., J. B.; Oliviera, A. C.; Gomes, F. A. A.; Myrabo, L. N.; Nagamatsu, H. T. (2007). New Hypersonic Shock Tunnel at the Laboratory of Aerothermodynamics and Hypersonics Prof. Henry T. Nagamatsu. Fifth International Symposium on Beamed Energy Propulsion. Kona, Hawai.

Yoler, Y.A. (1954). Hypersonic Shock Tube. California Institute of Technology. PhD Thesis.

9. RESPONSIBILITY NOTICE

The Authors are the only responsible for the printed material included in this scientific article.
The Authors declare that there is no conflict of interest regarding the publication of this scientific article.